journal of the mechanical behavior of biomedical materials 150 (2024) 106291

Contents lists available at ScienceDirect

Journal of the Mechanical Behavior of Biomedical Materials

journal homepage: www.elsevier.com/locate/jmbbm

Effect of the apron in the mechanical characterisation of hyperelastic materials by means of biaxial testing: A new method to improve accuracy

Sofia Di Leonardo [a], Alessandra Monteleone [a], Patrizia Caruso [a,b], Hugo Meecham-Garcia [c], Giuseppe Pitarresi [b], Gaetano Burriesci [a,c,*]

[a] Ri.MED Foundation, Palermo, Italy
[b] Engineering Department, University of Palermo, Italy
[c] UCL Mechanical Engineering, University College London, UK

ARTICLE INFO

Keywords:
Hyperelastic materials
Soft tissues testing protocol
Biaxial tensile testing
Digital image correlation
Non-linear finite element analysis
Mechanical characterisation methods

ABSTRACT

Biological soft tissues and polymers used in biomedical applications (e.g. in the cardiovascular area) are hyperelastic incompressible materials that commonly operate under multi-axial large deformation fields. Their characterisation requires biaxial tensile testing. Due to the typically small sample size, the gripping of the specimens commonly relies on rakes or sutures, where the specimen is punctured at the edges of the gauge area. This approach necessitates of an apron, excess of material around the gauge region.

This work analyses the apron influence on the estimated mechanical response of biaxial tests performed by using a rakes gripping system, with the aim of verifying the test accuracy and propose improved solutions.

In order to isolate the effect of the apron, avoiding the influence of anisotropy and inhomogeneity typical of most soft tissues, homogeneous and isotropic hyperplastic samples made from a uniform sheet of casted silicone were tested. The stress-strain response of specimens with different apron sizes/shapes was measured experimentally by means of biaxial testing and digital image correlation. Tests were replicated numerically, to interpret the experimental findings.

The apron surrounding the gauge area acts as an additional annular constraint which stiffens the system, resulting in a significant overestimate in the stress values. This error can be avoided by introducing specific cuts in the apron.

The study quantifies, for the first time, the correlation between the apron size/shape and the experimental stress overestimation, proposing a research protocol which, although identified on homogeneous hyperelastic materials, can be useful in providing more accurate characterisation of both, synthetic polymers and soft tissues.

1. Introduction

The accurate mechanical characterisation of biological soft tissues and elastomeric membranes is crucial for the understanding of cardiovascular biomechanics, the diagnosis of pathological situations, the design of in-vitro physiological models and the development therapeutic devices (Cowin and Humphrey, 2001; Ghanbari et al., 2009; Javani et al., 2016; Murdock et al., 2018; L'Acqua and Hod, 2015; Alekya et al., 2019; Martins et al., 2006; Miller, 2000; Wex et al., 2015).

Despite their different nature, biological soft tissues and elastomers share strong similarity in terms of macro-mechanical behaviour. Biological soft tissues are composed of bundles of collagen and elastin fibres, embedded in a ground substance (Raghupathy et al., 2011; Susan, 2015; Vignali et al., 2021). The coiled configuration and preferential alignment of the collagen fibres confer a non-linear, anisotropic and heterogeneous behaviour (Fung and Cowin, 1994; Sacks, 2000; Holzapfel, 2008; Jiang et al., 2021; Raghupathy et al., 2010); whilst the ground substance, essentially composed of water and large organic molecules, results in the incompressibility of the material (Ishihara et al., 1980; Di Puccio et al., 2012; Musotto et al., 2022; Guala et al., 2019). Elastomers are amorphous materials made of long polymeric chains chemically linked at various locations to form a stable network (Ali et al., 2010), which also exhibit non-linear nearly incompressible behaviour.

Both, biological tissues and elastomers used in biomedical applications (such as blood vessels, vascular grafts, heart valve leaflets and

* Corresponding author. Room 507A, Malet Place Engineering Building, Torrington Place, London, WC1E 7JE, UK.
E-mail address: g.burriesci@ucl.ac.uk (G. Burriesci).

https://doi.org/10.1016/j.jmbbm.2023.106291
Received 8 May 2023; Received in revised form 28 November 2023; Accepted 30 November 2023
Available online 4 December 2023

cardiac patches), typically operate under multi-axial loads and experience large elastic deformations, well above 10 % (El-Tallawi et al., 2021; Sobh et al., 2022; Satriano et al., 2018). Often, they are also characterised by the presence of some viscoelasticity and, eventually, plasticity (Islam et al., 2020; Schleip, 2003). Hyperelastic behaviours are commonly described by models that adopt strain energy function approaches, such as Neo-Hookean, Mooney-Rivlin and Ogden (Mooney, 1940; Rivlin and Rivlin, 1997; Ogden, 1972; Arruda and Boyce, 1993). These models can be integrated with springs and dashpots systems to simulate the viscoelastic behaviour (Maxwell, 1867; Shitikova and Krusser, 2022). This aspect, together with plasticity and anisotropy, is not investigated in this work.

The hyperelastic parameters defining the constitutive behaviour are determined from curve fitting of experimental data. However, parameters estimated for a specific deformation mode are often inadequate to correctly model other forms of deformation (Amin et al., 2006; Charlton et al., 1994). Hence, standard uniaxial tensile tests set for elastomeric materials (Standard, 1995; De Gelidi et al., 2016; Sokolis et al., 2002; Shergold et al., 2006; Robbins et al., 2020) are not suitable to define a material model experiencing the multi-axial large deformation that characterises the common operating conditions of soft tissues and elastomers in cardiovascular applications (Sacks et al., 2009; Rahmani et al., 2012, 2015; Ge et al., 2023; Bishnoi et al., 2015; Bourantas et al., 2019; Burriesci et al., 2010; Ono et al., 2023). These are more closely described by biaxial tests for which, however, standard guidelines have not been defined yet.

Where biaxial tensile tests can be performed on large specimens, cruciform shapes are preferred, with the arm ends fixed to the actuators through standard clamping. In this case, stress concentrations introduced at the gripped region dissipate along the arms, without introducing significant alterations in the central gauge area (Hartmann et al., 2018; Makris et al., 2010).

In the case of soft tissues, specimens are typically small (of the order of the centimetre) and inhomogeneous, so that it is normally impossible to adopt the cruciform configuration to obtain relevant parameters. Hence, square specimens of the available dimensions are used, and the load is applied at their edge portions through rakes or sutures permitting lateral deformation (Fehervary et al., 2016; Waldman et al., 2002; Sun et al., 2005; Avanzini and Battini, 2016). Rakes systems apply the load through a set of tines connected to beams anchored on a common base, and allow easy and repeatable mounting.

Cruciform specimens and rakes systems do not allow significant shear deformations, so that they are unsuitable for the characterisation of highly anisotropic materials, where the material axes can be easily aligned with the specimen sides. On the contrary, suture systems fix the specimen by using tethers mounted on pulleys, thus allowing the tethers to adjust their length to accommodate shear deformations and avoid the introduction of spurious shear stresses. However, their set up is very laborious and presents poor repeatability, often resulting in non-uniform load distributions (Fehervary et al., 2016).

Suture and rakes systems apply the load through punctures located in the proximity of the specimen edges. This necessarily requires some excess of material beyond the gauge area, whose minimum size depends on the suture retention strength of the material. This excess of material, normally called apron, is commonly assumed to have negligible effect on the strain map uniformity, although it is recognised that it may introduce some errors on stress estimation (Fehervary et al., 2016; Eilaghi et al., 2009).

In this work, the influence of the apron width on the mechanical behaviour is investigated experimentally and numerically, by performing biaxial tests on silicone specimens with different specimen dimensions. Silicone was chosen for its highly homogeneous and isotropic mechanical characteristics that help to isolate the apron width effect, and for its hyperelastic incompressible behaviour, which allows the direct extension of the findings from this study to soft tissues and generic elastomers. In particular, a set of specimens were tested in multiple stages, progressively reducing the width of the apron and then introducing cuts between the grips punctures to interrupt its continuity. The stress-strain behaviour was estimated for each test, obtaining the full field strain distribution by means of digital image correlation (DIC). The material response determined experimentally was then used to define the constitutive law in a finite element model which closely replicated the influence of the apron width as observed in the tests, allowing to examine the departure from the effective material behaviour and investigate alternative sample geometries that improve the test accuracy.

2. Materials and methods

2.1. Experimental set-up

Three square specimens made of GI-1100 bicomponent silicone (Silicones Inc., USA) of side 20 mm and thicknesses 1.20 mm, 0.94 mm and 0.92 mm, respectively, were prepared for mechanical biaxial testing. Tests were conducted on a CellScale Biotester (CellScale Biomaterials Testing, Canada). The testing machine applies the biaxial force through four actuators, instrumented with one load cells of 23 N per each loading direction, with an accuracy higher than 50 mN and sampling rate of 100 Hz. The system includes a high-resolution monochrome CCD camera for DIC analysis, with a resolution of 1280 × 960 pixels, and maximum acquisition rate of 15 frames per second. DIC is a contactless full-field technique that allows to obtain displacement and strain maps of the specimen surface under loading by means of subsets correlation (Sutton et al., 2009). Due to the uniformity of the specimen surface, a random black speckle was applied to the top face of the specimens to improve correlability (see Fig. 1).

Specimens were gripped using a rakes system BioRakes CS-BT-305-22-30, recommended for square specimen of side in the range 11.00–13.00 mm and providing a gauge area of 10 × 10 mm^2 (gauge length was 10 mm). Each rake comprises 5 tines of 0.305 mm diameter, equally spaced and an interaxial distance of 2.2 mm, allowing a maximum puncture depth of 1.9 mm.

In order to study the influence of the outer frame, each specimen was tested three times, progressively reducing the apron width from a maximum size of 50 % of the gauge length (A50) to 30 % (A30) and 10 % (A10) of the gauge length, respectively (see Fig. 2). Afterwards, in the A10 configuration, cuts between the tines were introduced, aligned with the rakes beams, and the four apron corners were removed, obtaining the trimmed specimen shape (T10) as shown in Fig. 2.

In order to modify the specimen apron without altering the attachment configuration, a rigid lifting plate was built (see Fig. 3a), allowing to perform the cutting procedure while maintaining the specimen firmly engaged on the rakes (see Fig. 3b). To cut the specimens, the plate was connected to the four rakes by screws serrated on dovetail pieces which allow to hold the rakes as shown in Fig. 3b. Once the rigid plate is connected to the four rakes, it allows to lift off the whole sample and rakes system and practice precise apron cutting/trimming with a scalpel. The modified specimen and the rakes can then be easily repositioned in the test position on the CellScale and disengaged from the lifting plate.

Each test was run under displacement control, applying a ramp from 0 to 2.5 mm at 0.1 mm/s, followed by a recovery to the initial position.

During the whole loading cycle, specimen pictures were acquired with a frequency of 5 Hz. DIC analysis was performed using the MATLAB open source code Ncorr (Blaber et al., 2015). Displacement and strain maps were obtained on a region of interest adjacent to the rakes, by setting a subset radius of 15–18 pixels, a subset spacing equal to 50 % of the subset radius and virtual strain gauge of 3, with a magnitude factor ranged between 0.008 and 0.012 mm/pixel.

For each test, true stress - true strain curves were obtained from the measured force assuming volume conservation (incompressibility), and determined from the equations below:

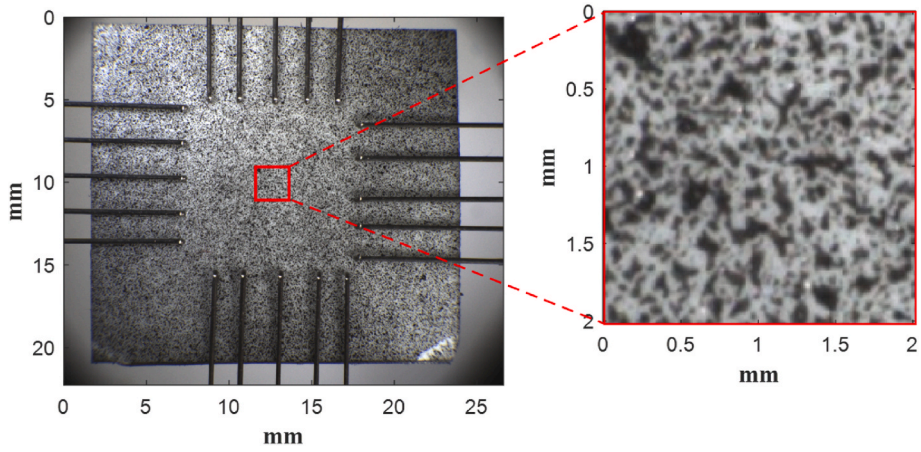

Fig. 1. Specimen clamped with a detail of the speckle.

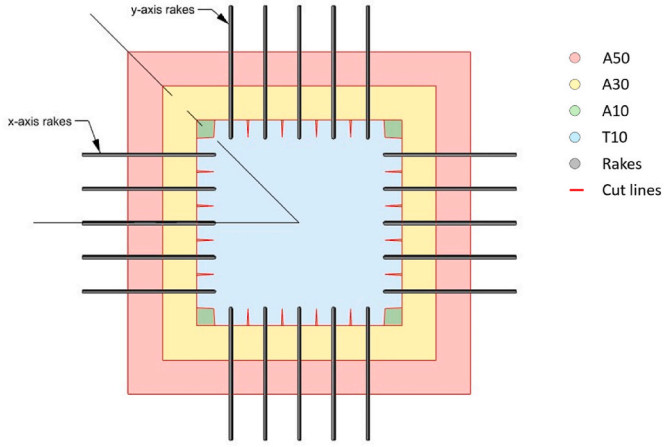

Fig. 2. Specimen cutting layout.

$$\sigma_{xx} = \frac{F_x\,(1+\varepsilon_{xx})}{l \cdot t} \tag{1}$$

$$\sigma_{yy} = \frac{F_y\,(1+\varepsilon_{yy})}{l \cdot t} \tag{2}$$

where F_x and F_y are the forces measured by the load cells in the x and y orientations, respectively; l is the gauge length and t is the initial thickness.; and ε_{xx} and ε_{yy} are the mean strain in x and y directions, measured in a central square region. In particular, a region of side equal to 30 % of the gauge length was analysed, where the stress concentrations introduced by the rakes at the punctures resulted negligible. Due to the isotropic behaviour of the silicone material, results in the x and y directions were averaged.

The resulting nominal stress-strain curves related to the T10 specimen were fitted with an Ogden model (Ogden, 1972; Holzapfel and Ogden, 2009), which is one of the most adopted incompressible hyperelastic models for the analysis of soft tissues and elastomers (Łagan and Liber-Kneć, 2017; Payne et al., 2015; Hadjicharalambous et al., 2015; Hajhosseini and Takalloozadeh, 2019; Asgari and Rashedi, 2018). Three terms of strain energy potential (3rd order formulation) was used, since it is reported to provide better agreement with elastomers test data than the Mooney-Rivlin or Neo Hookean alternative formulations (Kim et al., 2012), as in the following equation:

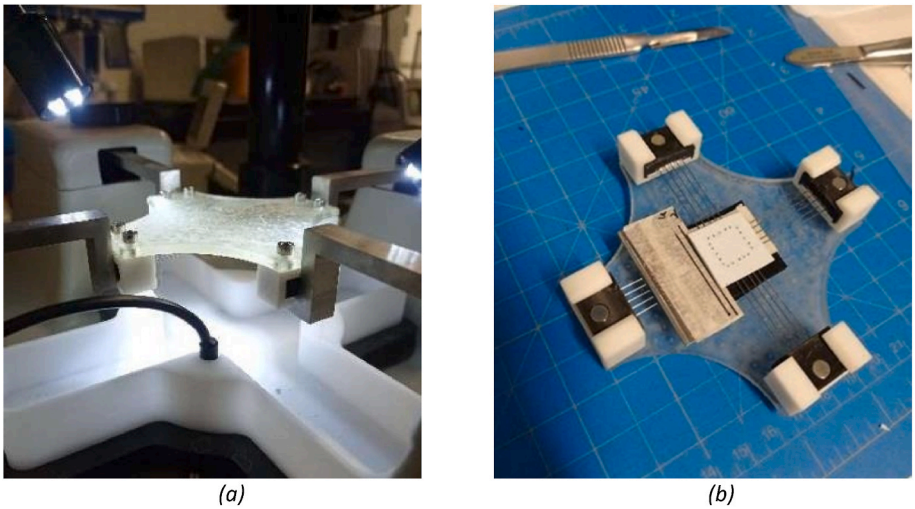

Fig. 3. A) Lifting system, b) Specimen cutting.

$$W_{Ogden} = \sum_{i=1}^{N} \frac{\mu_i}{\alpha_i} J^{\frac{-\alpha_i}{3}} \left(\lambda_1^{\alpha_i} + \lambda_2^{\alpha_i} + \lambda_3^{\alpha_i} - 3\right) \quad (3)$$

where J is the Jacobian measuring dilatancy, λ_1, λ_2 and λ_3 are the principal stretches, μ_i is a parameter descriptive of the shear modulus, α_i is a material constant, and N is the number of terms that defines the strain energy function. Constants μ_i and α_i obtained from the fitting procedure were used as input of the numerical simulations.

2.2. Simulation set-up

A finite element model of the square specimen tested biaxially with rakes systems was created in MSC.Marc/Mentat (MSC Software Corporation, 2016) to confirm the experimental findings, and support their interpretation. As shown in Fig. 4a, the symmetry of the specimen was exploited, modelling just one eighth of the whole geometry (Fig. 2) ,with a thickness of 1 mm. Holes of 0.305 mm diameter (equal to the tines diameter) were included in correspondence of the tines punctures. The A50 specimen model was meshed with about 40,400 eight-noded hexahedral elements (*hex 8 type 7* in MSC.Marc/Mentat (MSC Software Corporation, 2000)). As boundary conditions, symmetry was imposed on two planes (*Symmetry planes* in Fig. 4). Moreover, the central node of the upper surface was constrained in the z-direction. The specimen material was described with an Ogden material model, as discussed in the previous section 2.1. The A30 and A10 geometries were obtained from the A50 specimen model, by progressively erasing the elements at the edge to reduce the apron sizes as in the experiment (red, yellow and green regions in Fig. 4a). In the numerical study, an additional test with no apron (A0 in Fig. 4a) was performed, removing all apron elements. This is an ideal condition, practically unattainable, that can provide useful information by isolating the effect of the concentrated loading condition. The trimmed shape T10 was obtained from A10, by erasing the elements at the apron corners and disconnecting the elements neighbouring cuts by duplicating the interface nodes (see Fig. 4b). An additional numerical model, obtained applying the same approach on the A50, indicated as T50, was also analysed, to verify the effect of the apron width in trimmed specimens. This model could not be tested experimentally, as it was unattainable with the cutting sequence selected in the experiments. Table 1 summarises the denomination of each test specimen/model.

The tines were modelled as cylindrical structures of 0.305 mm diameter and 2 mm length, made from isotropic linear elastic steel (Young's modulus equal to 210 GPa and Poisson's ratio equal to 0.3). The nodes at their top and bottom ends were constrained in the z-direction.

Table 1
Denomination of each test specimen.

Denomination	Type of specimen/model
A50	Apron 50 % of gauge length
A30	Apron 30 % of gauge length
A10	Apron 10 % of gauge length
A0	Apron 0 % of gauge length
T10	Apron 10 % of gauge length with trims
T50	Apron 50 % of gauge length with trims

'Touching' type contact interaction was set between the specimen and the tines, with a friction coefficient of 0.3. As in the experimental tests, the load was applied by imposing on the tines a linearly increasing displacement in the x-direction, from 0 to 1.25 mm. The tines elements were left free to move in the y-direction, but rotations were prevented. Since for case A0 this loading scheme is not applicable (as there are no sample elements opposing the tines displacement), the elements of the specimen and tines were glued at their interface.

To compare the numerical results with the experimental ones, true stress - true strain curves were estimated as in the experiment. Specifically, true stress was obtained through equation (1), using the resultant of the contact force between the tines and the specimen (F_x). The strain was averaged over a central region of side equal to 30 % of the gauge length in the x-direction (ε_{xx}). For each simulation, the true stress - true strain curves were estimated as described above, and compared with the stress – strain curve extracted from the constitutive law used to define the material response. In particular, mean errors were evaluated as mean percentage difference of the stress at strains larger than 0.01 mm/mm.

3. Results

The strain maps of each specimen were evaluated at different instants of the loading cycle, by means of DIC analysis. The mean experimental nominal stress - strain curve obtained for the T10 specimens was fitted with the Ogden model with three terms ($N = 3$ in equation (3)), determining the following material constants: $\mu_1 = 0.0305268$ MPa, $\mu_2 = 0.765545$ MPa, $\mu_3 = 0.849083$ MPa and $\alpha_1 = 8.04226$, $\alpha_2 = 0.312771$, $\alpha_3 = 1.5235E\text{-}07$. These coefficients were used for the definition of the Ogden material in the numerical simulations.

In Fig. 5, the experimental and numerical strain maps are represented. For clarity and simplicity of representation, the experimental maps (Fig. 5a,c,e,h) are referred to one of the three specimens only (no significant differences were found among the three specimens). To facilitate comparison between experimental and computational results,

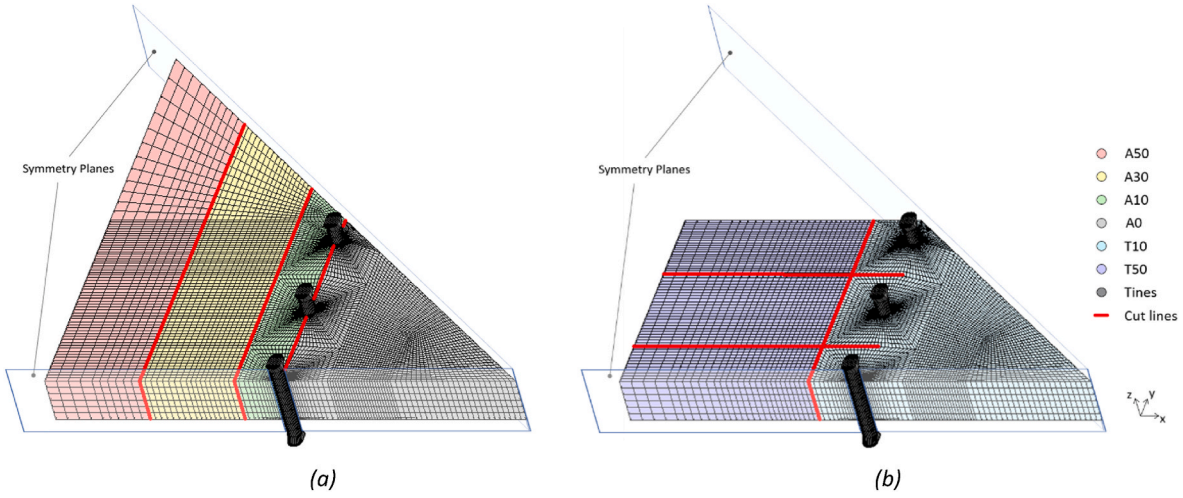

Fig. 4. Simulation design and mesh of: a) A50, A30, A10, A0; b) T10, T50 models.

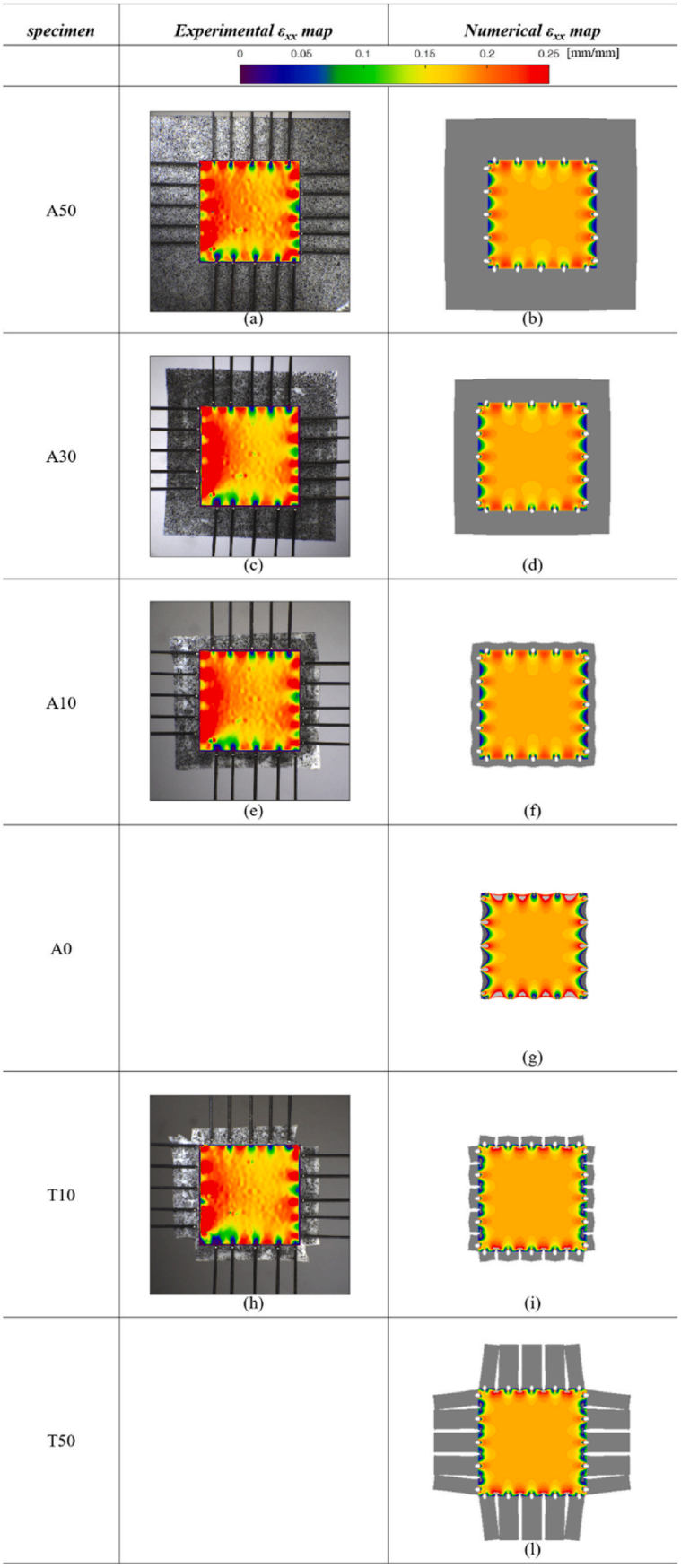

Fig. 5. ε_{xx} strain maps of experimental (left column) and numerical (right column) results for all cases: a,b) A50; c,d) A30; e,f) A10; g) A0; h,i) T10; l) T50.

numerical maps are only reported in the gauge area, displaying the apron in uniform grey colour. The experimental strain distribution in the central region appears reasonably uniform, independently of the apron width, with the maximum and minimum peaks of strain confined in proximity of the rakes punctures. Similar results are found for the respective numerical simulations (in Fig. 5b,d,f,i), although it appears clear that the extension of the central region, exhibiting uniform strain, expands with the reduction of the apron width. Similar strain maps are obtained for the trimmed specimens (Fig. 5i,l). The strain map related to the specimen with no apron A0 (Fig. 5g) presents uniform strain in the central region, with higher peaks of strain close to the tines.

True stress – true strain curves for all the apron width cases are reported in Fig. 6. The maximum strains measured in the central region are similar for all experimental cases (in Fig. 6a). This indicates that the effect of the apron width is not significant in the central region, and confirms that no relevant damage was introduced in the specimens during the multiple tests and manipulations. The stress values, instead, are different and decrease with the dimension of the apron, indicating a significant influence of the sample shape on the estimated rigidity. The curves obtained from the numerical simulations show the same trend (see Fig. 6b). In particular, tests show a progressively softer material response as the apron width reduces. Numerical simulations clearly indicate that this trend is associated with a more accurate estimate of the mechanical behaviour, which tends to approach the real material characteristic (dashed black line in Fig. 6b). Crucially, the accuracy of the prediction is significantly better for the two trimmed specimens (T10 and T50 in Fig. 6b), whose stress - strain curves appear well overlapped despite the very different size of the trimmed apron. It is interesting to observe that the T10 and T50 curves overlap with the A0 curve, confirming that the proposed trimmed procedure removes the apron effect.

The maximum stress values at equal strain reached for each configuration in the case of experimental and numerical simulations are reported in Table 2. Moreover, the mean errors are listed for the numerical simulation (second column of Table 2). Both the numerical and experimental results show a decreasing value of the maximum stress with the reduction of the apron width, as highlighted in Fig. 7.

The A0, T50 and T10 specimens present almost the same maximum stress, which is independent on the apron width and trimming procedure.

It is interesting to observe that the maximum stress determined experimentally on the specimens with large apron width experiences a small sudden drop at large strains due to an out of plane deflection of the apron. This is evident in the picture in Fig. 8. Due to the symmetry used in the numerical models, this phenomenon is not captured in the simulations.

Table 2
Maximum value of stress at equal strain and mean error between each specimen and the input curve.

Specimen	Maximum stress [MPa] (mean error [%])	
	Experimental	Numerical
A50	0.316 ± 0.022	0.356 (36 %)
A30	0.304 ± 0.028	0.331 (28 %)
A10	0.275 ± 0.023	0.289 (14 %)
A0	–	0.262 (4 %)
T10	0.250 ± 0.024	0.264 (4 %)
T50	–	0.262 (4 %)
Input	–	0.250

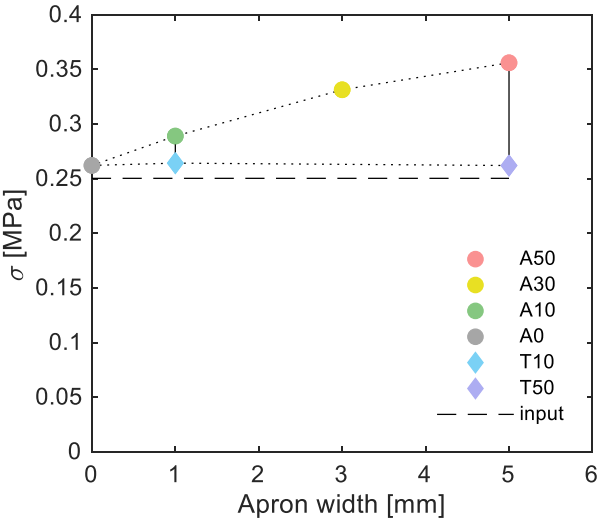

Fig. 7. Maximum true stress vs. apron width diagram for all the numerical results.

4. Discussion

Despite the growing relevance of biaxial tests for the characterisation of soft tissues and elastomers, not much research has been directed to the investigation and evaluation of the systematic errors affecting this type of assessment. Few studies have identified the apron as a potential source of error and focused on the analysis of its effect on the strain determination, concluding that this is negligible (Fehervary et al., 2016; Eilaghi et al., 2009).

In this work, the effect of the apron width on both the strain and

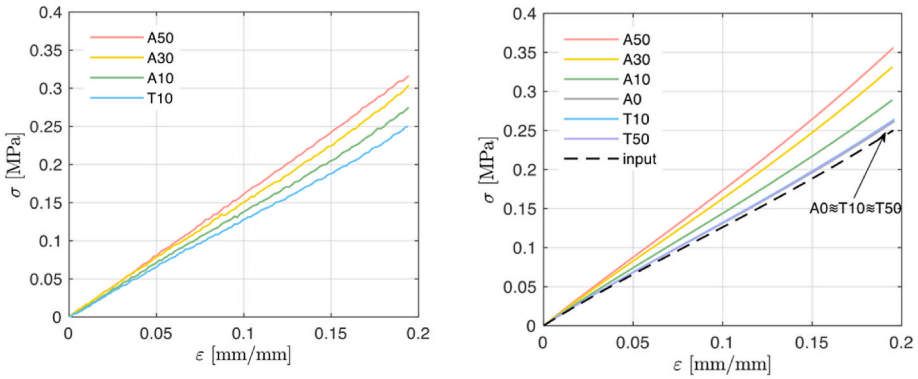

Fig. 6. True stress-true strain curves for all the a) experimental and b) numerical results.

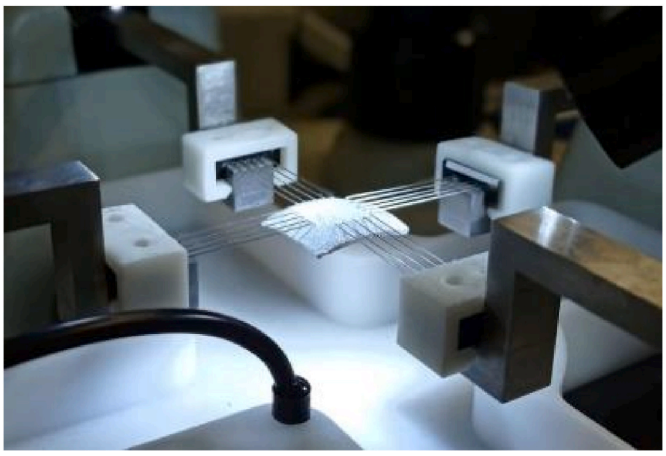

Fig. 8. A50 specimen bending during biaxial tensile test.

stress evaluation is investigated. Analysis of the strain distribution confirms that the apron width has small effect, although the reduction in the apron width results in an enlargement of the region characterised by a more uniform strain distributions at the centre of the specimen (as evident in Fig. 5). This can be useful when testing inhomogeneous materials, where the availability of larger areas with uniform strain distributions to perform averaging may provide a more significant characterisation.

On the other hand, the apron width has major influence on the stress, inducing very large errors on the stress measurement. In the analysed cases, these vary from 35 % for the A50 specimen to 14 % for the A10 specimen (denomination in Table 1). It is worth to mention that the latter is in the range of apron width recommended by the supplier of the test system. Smaller widths make very difficult to achieve a satisfactory centring of the specimen, and are likely to result into tearing at the anchoring punctures. Hence, the numerical analysis where the apron is totally removed (A0 specimen) is purely hypothetical, and has the function to verify the approximation introduced by the discontinuous loading. The loading modality is different for this model, with a pulling force acting directly at the inner semi-wall of the punctures. On the contrary, in the other models, the tines apply a compressive force on the external semi-wall of the punctures, causing ovalisation of the holes which results in some clearance at the inner side contact. Therefore, some difference in the strain distribution in proximity of the tines can be observed for the A0 model. This, however, is very confined and does not appear to affect the strain determined at the central region of the specimen. The absence of the apron strongly reduces the estimated stress values, containing the error in the determination of the stress within 5 %. This residual error is probably due to the presence of regions surrounding the punctures where the stress states are very different from equi-biaxial. In fact, as mentioned in the introduction, the parameters identified to define the hyperelastic behaviour from the biaxial test may be unsuitable to accurately capture the material response in these regions (Amin et al., 2006; Charlton et al., 1994). This suggests the impossibility to determine the real constitutive law from tests based on the use of rakes or sutures. However, errors below 5 % are usually well acceptable, especially in the characterisation of soft tissues, for which the intrinsic variability within the tissue and between samples is typically much larger than this error. Further studies on this issue will be needed to understand the influence of the different puncturing patterns and refine the gripping technique, where higher accuracies are needed.

The apron appears to acts as an annular constrain, which directly contributes to the force response of the specimen. Breaking the continuity of the apron with orthogonal trims (T10 and T50) is an effective solution, and produces identical behaviour and errors to the hypothetical case (A0) where the apron is totally removed. Hence, it allows to eliminate the error due to the presence of the apron, only retaining the error associated with the load discontinuity, which is normally acceptable.

The proposed trimming approach is very easy to implement and makes the characterisation independent of the apron size/shape. Hence, it can also be used to correct errors related to specimen centring and improper specimen cutting, providing more repeatable and consistent results. Also, it allows the testing of materials with poor suture retention, for which sufficient distance of the external margin from the anchoring puncture can be allowed, without increasing the error.

The trend observed in the experimental and numerical results is very similar, confirming that the proposed experimental approach, based on a trimmed specimen, allows to obtain an accurate material model. Some departure between the experimental behaviour and the numerical prediction becomes observable for the A50 specimen, at large stress levels. This can be attributed to an experimental artefact associated with the specific grip system. In fact, during loading, the offset R of the reaction force F of the specimen from the axis of the horizontal beam causes a bending of the rake beams and tines (see Fig. 9a) which promotes the out of plane deflection of the apron. This phenomenon, which is evident in Fig. 8, contributes to narrow the effective apron width, progressively reducing the slope of the stress-strain curve. The bending of the rake beams also produces an out of plane displacement of the specimen towards the camera. This, depending on the camera parallax, may be interpreted as an additional strain. Similarly, as the specimen stretches, the rake beams splay in the plane taking a folding fan shape, as depicted in Fig. 9b. Therefore, for large deformations, the component of the displacement of each tine of the same rake along the loading direction varies with their distance from the rake axis (they follow the dashed line in Fig. 9b).

All these factors, which cause the introduction of systematic errors in the experiment, were not simulated in the numerical analysis, in order to generalise the study without limiting it to a specific grip system. Specifically, the rake tines were modelled as cylinders unable to bend out of plane, which prevents the early instability of the apron leading to its out of plane deflection. Hence, the presented findings can be extended to other gripping systems, including sutures.

Contrary to the experimental procedure, where the specimen is punctured by the tines, the numerical models were created with holes of the same size as the tines. This does not model the presence of residual stresses generated by the perforation and expansion of the holes.

Finally, in order to reduce the effect of spurious actions and allow an easier interpretation of the phenomena, the study was performed on a specimen of constant thickness, made from a homogeneous and isotropic material. The effect of inhomogeneous and anisotropic materials, such as common soft tissues, will need to be verified in future studies.

5. Conclusions

The biaxial testing of soft tissues and elastomers often relies on gripping systems based on rakes and sutures, which require the presence of an apron in the specimen. This work has investigated the effect of this excess of material, combining experimental data assisted by DIC full-field analyses, supported by numerical simulations. The study has identified the apron as a major source of systematic error in the material characterisation. In particular, the apron directly contributes to the mechanical response of the specimen, producing a substantial overestimation of the stress. Reducing the apron width mitigates this effect, although practical constraints put a limit to the minimum attainable width, and to the possibility to minimise the error below one order of magnitude. A residual source of systematic error is identified in the discontinuity of the load, which is necessarily concentrated at specific locations (the punctures), locally departing from the equi-biaxial stress state. Hence, the mechanical characterisation by means of biaxial tests using rakes or sutures has an intrinsic limit in the accuracy, that is independent on the apron width.

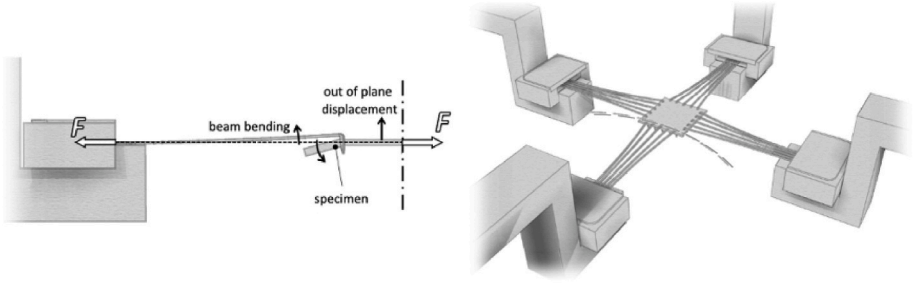

Fig. 9. Sketch of the experimental system with specimen and beams distortion: sagittal (a) and perspective (b) view.

In this work, a new solution is proposed, able to eliminate the error associated with the presence of the apron. This is of simple implementation, as it just requires the introduction of trims in the apron between the punctures, aligned with the direction of the load, and the removal of the apron corners. The solution appears to be effective, independently of the apron width and shape, allowing easy preparation and handling of the samples and adequate suture retention during testing.

Funding sources

This research did not receive any specific grant from funding agencies in the public, commercial, or not-for-profit sectors.

CRediT authorship contribution statement

Sofia Di Leonardo: Writing – original draft, Visualization, Validation, Software, Methodology, Investigation, Data curation, Conceptualization. **Alessandra Monteleone:** Writing – original draft, Visualization, Validation, Software, Methodology, Investigation, Data curation, Conceptualization. **Patrizia Caruso:** Methodology, Investigation, Data curation. **Hugo Meecham-Garcia:** Methodology, Investigation, Data curation. **Giuseppe Pitarresi:** Writing – review & editing, Visualization, Validation, Supervision, Resources, Project administration, Conceptualization. **Gaetano Burriesci:** Writing – review & editing, Visualization, Validation, Supervision, Resources, Project administration, Methodology, Investigation, Funding acquisition, Conceptualization.

Declaration of competing interest

The authors declare that they have no known competing financial interests or personal relationships that could have appeared to influence the work reported in this paper.

Data availability

Data will be made available on request.

References

Alekya, B., Sanjay, R., Pandya, H.J., 2019. Engineering approaches for characterizing soft tissue mechanical properties: a review. Clin. Biomech. 69, 127–140. https://doi.org/10.1016/j.clinbiomech.2019.07.016.

Ali, A., Hosseini, M., Sahari, B.B., 2010. A review of constitutive models for rubber-like materials. Am. J. Eng. Appl. Sci. 3, 232–239. https://doi.org/10.3844/ajeassp.2010.232.239.

Amin, A.F., Wiraguna, S.I., Bhuiyan, A.R., Okui, Y., 2006. Hyperelasticity model for finite element analysis of atural and high damping rubbers in compression and shear. J. Eng. Mech. 132, 54–64.doi:10.1061/(ASCE)0733-9399(2006)132:1(54).

Arruda, E.M., Boyce, M.C., 1993. A three-dimensional constitutive model for the large stretch behavior of rubber elastic materials. J. Mech. Phys. Solid. 41, 389–412. https://doi.org/10.1016/0022-5096(93)90013-6.

Asgari, M., Rashedi, B., 2018. Pertinence of sheep knee joint for calibration of ligaments' constitutive equations; experimental and theoretical study. Aut J. Mech. Eng. doi.org/10.22060/ajme.2018.13821.5322.

Avanzini, A., Battini, D., 2016. Integrated experimental and numerical comparison of different approaches for planar biaxial testing of a hyperelastic material. Adv. Mater. Sci. Eng. 1–12. https://doi.org/10.1155/2016/6014129, 2016.

Bishnoi, R.N., Jones, T.K., Kreutzer, J., Ringel, R.E., 2015. NuMED covered cheatham-platinum stent^{TM} for the treatment or prevention of right ventricular outflow tract conduit disruption during transcatheter pulmonary valve replacement, Catheter. Cardiovasc. Interv. 85, 421–427. https://doi.org/10.1002/ccd.25682.

Blaber, J., Adair, B., Antoniou, A., 2015. Ncorr: open-source 2D digital image correlation matlab software. Exp. Mech. 55, 1105–1122. https://doi.org/10.1007/s11340-015-0009-1.

Bourantas, C.V., Modolo, R., Baumbach, A., Søndergaard, L., Prendergast, B.D., Ozkor, M., Kennon, S., Mathur, A., Mullen, M.J., Serruys, P.W., 2019. The evolution of device technology in transcatheter aortic valve implantation. EuroIntervention 14, e1826–e1833. https://doi.org/10.4244/EIJ-D-18-01048.

Burriesci, G., Marincola, F.C., Zervides, C., 2010. Design of a novel polymeric heart valve. J. Med. Eng. Technol. 34, 7–22. https://doi.org/10.3109/03091900903261241.

Charlton, D.J., Yang, J., Teh, K.K., 1994. A review of methods to characterize rubber elastic behavior for use in finite element analysis. Rubber Chem. Technol. 67, 481–503. https://doi.org/10.5254/1.3538686.

Cowin, S.C., Humphrey, J.D., 2001. Cardiovascular Soft Tissue Mechanics, p. 259. https://doi.org/10.1007/0-306-48389-0.

De Gelidi, S., Tozzi, G., Bucchi, A., 2016. The role of pre-conditioning frequency in the experimental characterization of hyper-elastic materials as models for soft tissue applications. Int. J. Appl. Mech. 8 https://doi.org/10.1142/S1758825116500666.

Di Puccio, F., Celi, S., Forte, P., 2012. Review of experimental investigations on compressibility of arteries and introduction of a new apparatus. Exp. Mech. 52, 895–902. https://doi.org/10.1007/s11340-012-9614-4.

Eilaghi, A., Flanagan, J.G., Brodland, G.W., Ethier, C.R., 2009. Strain uniformity in biaxial specimens is highly sensitive to attachment details. J. Biomech. Eng. 131 https://doi.org/10.1115/1.3148467.

El-Tallawi, K.C., Zhang, P., Azencott, R., He, J., Herrera, E.L., Xu, J., Chamsi-Pasha, M., Jacob, J., Lawrie, G.M., Zoghbi, W.A., 2021. Valve strain quantitation in normal mitral valves and mitral prolapse with variable degrees of regurgitation. JACC Cardiovasc. Imaging 14, 1099–1109. https://doi.org/10.1016/j.jcmg.2021.01.006.

Fehervary, H., Smoljkić, M., Vander Sloten, J., Famaey, N., 2016. Planar biaxial testing of soft biological tissue using rakes: a critical analysis of protocol and fitting process. J. Mech. Behav. Biomed. Mater. 61, 135–151. https://doi.org/10.1016/j.jmbbm.2016.01.011.

Fung, Y.C., Cowin, S.C., 1994. Biomechanics: mechanical properties of living tissues, 2nd ed. J. Appl. Mech. 61 https://doi.org/10.1115/1.2901550, 1007–1007.

Ge, J., Zhou, D., Zhang, X., Hou, S., Chen, S., Jin, Q., Pan, W., Li, W., Pan, C., Qian, J., 2023. Preliminary implantation of a novel TAVR device with polymeric leaflets for symptomatic calcific aortic disease. JACC Case Reports 17, 101901. https://doi.org/10.1016/j.jaccas.2023.101901.

Ghanbari, H., Viatge, H., Kidane, A.G., Burriesci, G., Tavakoli, M., Seifalian, A.M., 2009. Polymeric heart valves: new materials, emerging hopes. Trends Biotechnol. 27, 359–367. https://doi.org/10.1016/j.tibtech.2009.03.002.

Guala, A., Teixidó-Tura, G., Rodríguez-Palomares, J., Ruiz-Muñoz, A., Dux-Santoy, L., Villalva, N., Granato, C., Galian, L., Gutiérrez, L., González-Alujas, T., Sanchez, V., Forteza, A., García-Dorado, D., Evangelista, A., 2019. Proximal aorta longitudinal strain predicts aortic root dilation rate and aortic events in Marfan syndrome. Eur. Heart J. 40, 2047–2055. https://doi.org/10.1093/eurheartj/ehz191.

Hadjicharalambous, M., Chabiniok, R., Asner, L., Sammut, E., Wong, J., Carr-White, G., Lee, J., Razavi, R., Smith, N., Nordsletten, D., 2015. Analysis of passive cardiac constitutive laws for parameter estimation using 3D tagged MRI. Biomech. Model. Mechanobiol. 14, 807–828. https://doi.org/10.1007/s10237-014-0638-9.

Hajhosseini, P., Takalloozadeh, M., 2019. An isotropic hyperelastic model of esophagus tissue layers along with three-dimensional simulation of esophageal peristaltic behavior. J. Bioeng. Res. https://doi.org/10.22034/JBR.2019.189018.1009.

Hartmann, S., Gilbert, R.R., Sguazzo, C., 2018. Basic studies in biaxial tensile tests. GAMM-Mitteilungen 41, e201800004. https://doi.org/10.1002/gamm.201800004.

Holzapfel, G., 2008. Collagen in Arterial Walls: Biomechanical Aspects. Springer US, Boston, MA, n.d, pp. 285–324. https://doi.org/10.1007/978-0-387-73906-9_11.

Holzapfel, G.A., Ogden, R.W., 2009. Constitutive modelling of passive myocardium: a structurally based framework for material characterization. Philos. Trans. R. Soc. A Math. Phys. Eng. Sci. 367, 3445–3475. https://doi.org/10.1098/rsta.2009.0091.

Ishihara, T., Ferrans, V.J., Jones, M., Boyce, S.W., Kawanami, O., Roberts, W.C., 1980. Histologic and ultrastructural features of normal human parietal pericardium. Am. J. Cardiol. 46, 744–753. https://doi.org/10.1016/0002-9149(80)90424-5.

Islam, M.R., Virag, J., Oyen, M.L., 2020. Micromechanical poroelastic and viscoelastic properties of ex-vivo soft tissues. J. Biomech. 113, 110090 https://doi.org/10.1016/j.jbiomech.2020.110090.

Javani, S., Gordon, M., Azadani, A.N., 2016. Biomechanical properties and microstructure of heart chambers: a paired comparison study in an ovine model. Ann. Biomed. Eng. 44, 3266–3283. https://doi.org/10.1007/s10439-016-1658-7.

Jiang, M., Sridhar, R.L., Robbins, A.B., Freed, A.D., Moreno, M.R., 2021. A versatile biaxial testing platform for soft tissues. J. Mech. Behav. Biomed. Mater. 114, 104144 https://doi.org/10.1016/j.jmbbm.2020.104144.

Kim, B., Lee, S.B., Lee, J., Cho, S., Park, H., Yeom, S., Park, S.H., 2012. A comparison among Neo-Hookean model, Mooney-Rivlin model, and Ogden model for chloroprene rubber. Int. J. Precis. Eng. Manuf. 13, 759–764. https://doi.org/10.1007/s12541-012-0099-y.

Łagan, S.D., Liber-Kneć, A., 2017. Experimental testing and constitutive modeling of the mechanical properties of the swine skin tissue. Acta Bioeng. Biomech. 19, 93–102. https://doi.org/10.5277/ABB-00755-2016-02.

L'Acqua, C., Hod, E., 2015. New perspectives on the thrombotic complications of haemolysis. Br. J. Haematol. 168, 175–185. https://doi.org/10.1111/bjh.13183.

Makris, A., Vandenbergh, T., Ramault, C., Van Hemelrijck, D., Lamkanfi, E., Van Paepegem, W., 2010. Shape optimisation of a biaxially loaded cruciform specimen. Polym. Test. 29, 216–223. https://doi.org/10.1016/j.polymertesting.2009.11.004.

Martins, P.A.L.S., Natal Jorge, R.M., Ferreira, A.J.M., 2006. A comparative study of several material models for prediction of hyperelastic properties: application to silicone-rubber and soft tissues. Strain 42, 135–147. https://doi.org/10.1111/j.1475-1305.2006.00257.x.

Maxwell, J., 1867. IV. On the dynamical theory of gases. Philos. Trans. R. Soc. London, A 157, 49–88. https://doi.org/10.1098/rstl.1867.0004.

Miller, K., 2000. Biomechanics of soft tissues. Med. Sci. Mon. Int. Med. J. Exp. Clin. Res. 6 https://doi.org/10.1016/b978-012443341-0/50107-1.

Mooney, M., 1940. A theory of large elastic deformation. J. Appl. Phys. 11, 582–592. https://doi.org/10.1063/1.1712836.

MSC Software Corporation, 2000. MSC.Marc Volume B. Element Library. http://www.sd.rub.de/downloads/links/marc_manuals/online_documentation_marc_2000/volb/volb.pdf.

MSC Software Corporation, 2016. MSC Marc Theory and User Information, Msc, pp. 82–85. Software, Palo Alto, USA. http://scholar.google.com/scholar?hl=en&btnG=Search&q=intitle:Volume+A+:+Theory+and+User+Information#0.

Murdock, K., Martin, C., Sun, W., 2018. Characterization of mechanical properties of pericardium tissue using planar biaxial tension and flexural deformation. J. Mech. Behav. Biomed. Mater. 77, 148–156. https://doi.org/10.1016/j.jmbbm.2017.08.039.

Musotto, G., Monteleone, A., Vella, D., Di Leonardo, S., Viola, A., Pitarresi, G., Zuccarello, B., Pantano, A., Cook, A., Bosi, G.M., Burriesci, G., 2022. The role of patient-specific morphological features of the left atrial appendage on the thromboembolic risk under atrial fibrillation. Front. Cardiovasc. Med. 9 https://doi.org/10.3389/fcvm.2022.894187.

Ogden, R.W., 1972. Large deformation isotropic elasticity – on the correlation of theory and experiment for incompressible rubberlike solids. Proc. R. Soc. London. A. Math. Phys. Sci. 326, 565–584. https://doi.org/10.1098/rspa.1972.0026.

Ono, M., Kageyama, S., O'Leary, N., El-Kurdi, M.S., Reinöhl, J., Solien, E., Bianco, R.W., Doss, M., Meuris, B., Virmani, R., Cox, M., Onuma, Y., Serruys, P.W., 2023. 1-Year patency of biorestorative polymeric coronary artery bypass grafts in an ovine model, JACC basic to transl. Sci 8, 19–34. https://doi.org/10.1016/j.jacbts.2022.06.021.

Payne, T., Mitchell, S., Bibb, R., Waters, M., 2015. Development of novel synthetic muscle tissues for sports impact surrogates. J. Mech. Behav. Biomed. Mater. 41, 357–374. https://doi.org/10.1016/j.jmbbm.2014.08.011.

Raghupathy, R., Barocas, V.H., Ishihara, T., Ferrans, V.J., Jones, M., Boyce, S.W., Kawanami, O., Roberts, W.C., Avanzini, A., Battini, D., Wright, S.F., Zadrazil, I., Markides, C.N., Meichner, C., Schedl, A.E., Neuber, C., Kreger, K., Schmidt, H.W., Kador, L., Lanir, Y., Fung, Y.C.C., Fan, R., Sacks, M.S., Yousif, M.Y., Holdsworth, D. W., Poepping, T.L., Aggarwal, A., Lombardi, D., Pant, S., Murdock, K., Martin, C., Sun, W., Nolan, D.R., McGarry, J.P., Raghupathy, R., Barocas, V.H., Sun, W., Sacks, M.S., Scott, M.J., Xiao, H., Lu, J., Qiu, H., Li, Y., Raghupathy, R., Witzenburg, C., Lake, S.P., Sander, E.A., Barocas, V.H., O'Leary, S.A., Doyle, B.J., McGloughlin, T.M., Fehervary, H., Smoljkić, M., Vander Sloten, J., Famaey, N., Manual, B.U., Vignali, E., Gasparotti, E., Landini, L., Celi, S., Rehman, I., Rehman, A., De Gelidi, S., Tozzi, G., Bucchi, A., Javani, S., Gordon, M., Azadani, A.N., Di Martino, E.S., Bellini, C., Schwartzman, D.S., Zhang, W., Feng, Y., Lee, C.H., Billiar, K.L., Michael, S., Jiang, M., Sridhar, R.L., Robbins, A.B., Freed, A.D., Moreno, M.R., Sacks, M.S., Fung, Y.C.C., Cowin, S.C., 2010. Generalized anisotropic inverse mechanics for soft tissues. J. Biomech. Eng. 132, 29–34. https://doi.org/10.1115/1.4001257.

Raghupathy, R., Witzenburg, C., Lake, S.P., Sander, E.A., Barocas, V.H., 2011. Identification of regional mechanical anisotropy in soft tissue analogs. J. Biomech. Eng. 133 https://doi.org/10.1115/1.4005170.

Rahmani, B., Cousins, B.G., Burriesci, G., Seifalian, A.M., 2015.Heart. Valves, Polymeric: Biocompatibility. Encycl. Biomed. Polym. Polym. Biomater.

Rahmani, B., Tzamtzis, S., Ghanbari, H., Burriesci, G., Seifalian, A.M., 2012. Manufacturing and hydrodynamic assessment of a novel aortic valve made of a new nanocomposite polymer. J. Biomech. 45, 1205–1211. https://doi.org/10.1016/j.jbiomech.2012.01.046.

Rivlin, R.S., 1997. Large elastic deformations of isotropic materials. In: Rivlin, R.S. (Ed.), Collect. Pap. Springer New York, New York, NY, pp. 90–108. https://doi.org/10.1007/978-1-4612-2416-7_8.

Robbins, A.B., Freed, A.D., Moreno, M.R., 2020. Characterizing the non-linear mechanical behavior of native and biomimetic engineered tissues in 1D with physically meaningful parameters. J. Mech. Behav. Biomed. Mater. 102, 103509 https://doi.org/10.1016/j.jmbbm.2019.103509.

Sacks, M.S., 2000. Biaxial mechanical evaluation of planar biological materials. J. Elast. 61, 199–246. https://doi.org/10.1023/A:1010917028671.

Sacks, M.S., David Merryman, W., Schmidt, D.E., 2009. On the biomechanics of heart valve function. J. Biomech. 42 https://doi.org/10.1016/j.jbiomech.2009.05.015.

Satriano, A., Guenther, Z., White, J.A., Merchant, N., Di Martino, E.S., Al-Qoofi, F., Lydell, C.P., Fine, N.M., 2018. Three-dimensional thoracic aorta principal strain analysis from routine ECG-gated computerized tomography: feasibility in patients undergoing transcatheter aortic valve replacement. BMC Cardiovasc. Disord. 18, 76. https://doi.org/10.1186/s12872-018-0818-0.

Schleip, R., 2003. Fascial plasticity – a new neurobiological explanation: Part 1. J. Bodyw. Mov. Ther. 7, 11–19. https://doi.org/10.1016/S1360-8592(02)00067-0.

Shergold, O.A., Fleck, N.A., Radford, D., 2006. The uniaxial stress versus strain response of pig skin and silicone rubber at low and high strain rates. Int. J. Impact Eng. 32, 1384–1402. https://doi.org/10.1016/j.ijimpeng.2004.11.010.

Shitikova, M.V., Krusser, A.I., 2022. Models of Viscoelastic Materials: A Review on Historical Development and Formulation, pp. 285–326. https://doi.org/10.1007/978-3-031-04548-6_14.

Sobh, D.M., Tawfik, A.M., Batouty, N.M., Sobh, H.M., Hamdy, N., Bakr, A., Eid, R., Awad, M.H., Gadelhak, B., 2022. Impaired aortic strain and distensibility by cardiac MRI in children with chronic kidney disease. Sci. Rep. 12, 11079 https://doi.org/10.1038/s41598-022-15017-9.

Sokolis, D.P., Boudoulas, H., Karayannacos, P.E., 2002. Assessment of the aortic stress-strain relation in uniaxial tension. J. Biomech. 35 https://doi.org/10.1016/S0021-9290(02)00073-8.

Standard, BS 903-5, 1995. Physical Testing of Rubber. Part 1: Guide to the Selection and Use of Methods of Test for Rubber.

Sun, W., Sacks, M.S., Scott, M.J., 2005. Effects of boundary conditions on the estimation of the planar biaxial mechanical properties of soft tissues. J. Biomech. Eng. 127, 709–715. https://doi.org/10.1115/1.1933931.

Susan, P., 2015. Standring DSc, Gray's Anatomy. The Anatomical Basis of Clinical Practice.

Sutton, M.A., Orteu, J.J., Schreier, H.W., 2009. Image Correlation for Shape, Motion and Deformation Measurements. Springer US, Boston, MA. https://doi.org/10.1007/978-0-387-78747-3.

Vignali, E., Gasparotti, E., Landini, L., Celi, S., 2021. Development and realization of an experimental bench test for synchronized small angle light scattering and biaxial traction analysis of tissues. Electron 10, 1–16. https://doi.org/10.3390/electronics10040386.

Waldman, S.D., Sacks, M.S., Lee, J.M., 2002. Boundary conditions during biaxial testing of planar connective tissues: Part II. Fiber orientation. J. Mater. Sci. Lett. 21, 1215–1221. https://doi.org/10.1023/A:1016576603938.

Wex, C., Arndt, S., Stoll, A., Bruns, C., Kupriyanova, Y., 2015. Isotropic incompressible hyperelastic models for modelling the mechanical behaviour of biological tissues: a review. Biomed. Eng./Biomed. Tech. 60 https://doi.org/10.1515/bmt-2014-0146.